# Common path in-line holography using enhanced joint object reference digital interferometers

**Roy Kelner,[1,*] Barak Katz,[1,2] and Joseph Rosen[1,3]**

[1]*Department of Electrical and Computer Engineering, Ben-Gurion University of the Negev, P.O. Box 653, Beer-Sheva 8410501, Israel*
[2]*barakk@ee.bgu.ac.il*
[3]*rosen@ee.bgu.ac.il*
[*]*kelnerr@post.bgu.ac.il*

**Abstract:** Joint object reference digital interferometer (JORDI) is a recently developed system capable of recording holograms of various types [Opt. Lett. **38**(22), 4719 (2013)]. Presented here is a new enhanced system design that is based on the previous JORDI. While the previous JORDI has been based purely on diffractive optical elements, displayed on spatial light modulators, the present design incorporates an additional refractive objective lens, thus enabling hologram recording with improved resolution and increased system applicability. Experimental results demonstrate successful hologram recording for various types of objects, including transmissive, reflective, three-dimensional, phase and highly scattering objects. The resolution limit of the system is analyzed and experimentally validated. Finally, the suitability of JORDI for microscopic applications is verified as a microscope objective based configuration of the system is demonstrated.



**OCIS codes:** (090.0090) Holography; (090.1995) Digital holography; (090.1760) Computer holography; (110.6880) Three-dimensional image acquisition; (100.3010) Image reconstruction techniques; (070.6120) Spatial light modulators; (180.6900) Three-dimensional microscopy; (090.2880) Holographic interferometry; (090.1970) Diffractive optics.

## References and links

1. Y. Rivenson, B. Katz, R. Kelner, and J. Rosen, "Single channel in-line multimodal digital holography," Opt. Lett. **38**(22), 4719–4722 (2013).
2. B. Katz, J. Rosen, R. Kelner, and G. Brooker, "Enhanced resolution and throughput of Fresnel incoherent correlation holography (FINCH) using dual diffractive lenses on a spatial light modulator (SLM)," Opt. Express **20**(8), 9109–9121 (2012).
3. D. Gabor, "A new microscopic principle," Nature **161**(4098), 777–778 (1948).
4. E. N. Leith and J. Upatnieks, "Reconstructed wavefronts and communication theory," J. Opt. Soc. Am. **52**(10), 1123–1128 (1962).
5. I. Yamaguchi and T. Zhang, "Phase-shifting digital holography," Opt. Lett. **22**(16), 1268–1270 (1997).
6. V. Micó, J. García, Z. Zalevsky, and B. Javidi, "Phase-shifting Gabor holography," Opt. Lett. **34**(10), 1492–1494 (2009).
7. V. Linnik, "Simple interferometer for the investigation of optical systems," Proc. Acad. Sci. USSR **1**, 208–210 (1933).
8. R. N. Smartt and W. H. Steel, "Theory and application of point-diffraction interferometers," Jpn. J. Appl. Phys. **14**, 351–357 (1975).
9. H. Kadono, N. Takai, and T. Asakura, "New common-path phase shifting interferometer using a polarization technique," Appl. Opt. **26**(5), 898–904 (1987).
10. C. Ramírez, E. Otón, C. Iemmi, I. Moreno, N. Bennis, J. M. Otón, and J. Campos, "Point diffraction interferometer with a liquid crystal monopixel," Opt. Express **21**(7), 8116–8125 (2013).
11. J. Garcia-Sucerquia, W. Xu, S. K. Jericho, P. Klages, M. H. Jericho, and H. J. Kreuzer, "Digital in-line holographic microscopy," Appl. Opt. **45**(5), 836–850 (2006).

#204375 - $15.00 USD Received 8 Jan 2014; revised 11 Feb 2014; accepted 13 Feb 2014; published 24 Feb 2014

12. O. Mudanyali, D. Tseng, C. Oh, S. O. Isikman, I. Sencan, W. Bishara, C. Oztoprak, S. Seo, B. Khademhosseini, and A. Ozcan, "Compact, light-weight and cost-effective microscope based on lensless incoherent holography for telemedicine applications," Lab Chip **10**(11), 1417–1428 (2010).
13. V. Arrizón and D. Sánchez-de-la-Llave, "Common-path interferometry with one-dimensional periodic filters," Opt. Lett. **29**(2), 141–143 (2004).
14. V. Mico, Z. Zalevsky, and J. García, "Superresolution optical system by common-path interferometry," Opt. Express **14**(12), 5168–5177 (2006).
15. P. Gao, G. Pedrini, and W. Osten, "Structured illumination for resolution enhancement and autofocusing in digital holographic microscopy," Opt. Lett. **38**(8), 1328–1330 (2013).
16. R. Kelner, J. Rosen, and G. Brooker, "Enhanced resolution in Fourier incoherent single channel holography (FISCH) with reduced optical path difference," Opt. Express **21**(17), 20131–20144 (2013).
17. R. Kelner and J. Rosen, "Spatially incoherent single channel digital Fourier holography," Opt. Lett. **37**(17), 3723–3725 (2012).
18. O. Bryngdahl and A. Lohmann, "Variable magnification in incoherent holography," Appl. Opt. **9**(1), 231–232 (1970).
19. D. N. Naik, G. Pedrini, and W. Osten, "Recording of incoherent-object hologram as complex spatial coherence function using Sagnac radial shearing interferometer and a Pockels cell," Opt. Express **21**(4), 3990–3995 (2013).
20. B. Katz and J. Rosen, "Super-resolution in incoherent optical imaging using synthetic aperture with Fresnel elements," Opt. Express **18**(2), 962–972 (2010).
21. J. W. Goodman, *Introduction to Fourier Optics* (McGraw-Hill, 1996), Chap. 8, p. 273 and Chap. 5, p. 97.
22. M. Born and E. Wolf, *Principles of Optics* (Cambridge, 1999), Chap. 8.6.3, p. 471.

## 1. Introduction

Recently, the joint object reference digital interferometer (JORDI) has been introduced as a system for recording digital holograms of various types under coherent illumination [1]. In JORDI, hologram formation is accomplished through the interference of two distinctively different parts of the same input beam: one that contains the object (or scene) scattered information, and another unscattered part. The latter does not contain any object related information, and can thus be used as a source for the reference beam. The actual interference between the object and reference parts is made possible through the utilization of the birefringence properties of liquid crystal spatial light modulators (SLMs), by which orthogonal polarization components of the input beam can be optically manipulated in different ways. These manipulations enable hologram recording using a digital camera, upon which an imaging of the object scattered information is made to overlap with a reference beam. The use of SLMs offers flexibility, and holograms of several modalities (including off-axis and on-axis phase-shifting Fresnel holograms, and image holograms) can easily be recorded [1]. The combination of the polarization dependent control and the presence of both object and reference information at the same input wave (i.e., joint object reference) enables the realization of JORDI in a single-channel, common-path configuration. This holds the advantages of offering system robustness due to inherent resistance to vibrations, easier assembly and alignment of the optical system, and can possibly allow the recording of temporally incoherent holograms, as long as the optical path difference (OPD) between interfering beams is small enough [2].

In retrospect, it is not surprising that the first ever holographic setup, invented by Gabor [3], was realized by a single channel configuration. However, two significant issues restrict the usability of Gabor's original implementation. The first is the well-known twin image problem, where two conjugated images are formed for a single recorded object and together with an additional 0th diffraction order term undermine the quality and the visibility of the holographic reconstruction. The second is the weak-scattering condition which restricts the hologram recording to objects that must emit two mutually coherent waves: one that is much more intense than the other, but does not carry any spatial information, and another that contains the information in a form of a scattering, low intensity beam. Luckily, solutions for solving these issues have been proposed throughout the years; the most famous one is the off-axis holography suggested by Leith and Upatnieks [4]. Other approaches maintain the single channel configuration and adopt a phase-shifting procedure [5] for the removal of the twin-image and bias (0th order) term. For example, Mico et al. [6] propose the "phase-shifting

#204375 - $15.00 USD Received 8 Jan 2014; revised 11 Feb 2014; accepted 13 Feb 2014; published 24 Feb 2014

Gabor holography" method where an SLM replaces the usual semi-transparent pinhole slide found in the point-diffraction interferometer (PDI) [7,8], and the central pixel of the SLM is used for phase-shifting the non-scattering light of the input target . This non-scattering term, in turn, serves as the reference of the recorded hologram. A similar approach for phase-shifting had been suggested before [9], but required a mechanical intervention between exposures. Recently, a more economical implementation of the phase-shifting PDI using a mono-pixel SLM has been proposed [10].

Though the twin-image problem in PDI is easily resolved via phase-shifting, under high scattering conditions the non-scattering term might prove too weak relative to other diffracted terms, limiting hologram recording due to an insufficient visibility of the interference fringes. Alternative approaches to single-channel holography remedy this issue by ensuring that a large enough portion of the illumination freely passes around the object (see, e.g., [11] where coherent illumination is used, and [12] where a very compact design of the optical apparatus enables the use of a light source of a lesser degree of spatial and temporal coherence), or demand either a separation [13] or coexistence [1] of the object and reference within the system input plane. In [13] the interference between the reference and object originated waves is achieved through the use of a diffraction grating, a concept that has successfully been used later for achieving super-resolution holography via either off-axis [14] or structured [15] illumination.

In JORDI, one may consider the hologram recording as a result of the combination of lateral and radial shearing, where the object part of the input beam is made to overlap with the reference part of the same input beam. The object and reference parts undergo different magnifications (attributed to the radial shearing), and additional lateral shearing is applied (whenever necessary) to the reference part so that the two parts overlap at the hologram plane. Interestingly, similar concepts were used for the successful realization of spatially incoherent holography. For example, in a recent publication [16] we have shown how the Fourier incoherent single channel holography system [17] can be considered as a combination of both rotational and radial shearing interferometers. Other examples are described in [18,19] where incoherent Fourier hologram are recorded using a radially shearing Sagnac interferometer, which is an example of a dual-channel common-path configuration. Note that the systems in [16–19] are self-referencing in nature, and unlike JORDI do not require separate object and reference parts. In such systems, the recorded hologram represents the summation over all point source contributions, as many self-interferences occur in parallel. In the former JORDI implementation [1], the above mentioned radial and lateral shearing was achieved by the use of each of the two SLMs as a single lens imaging system, offering simplicity and flexibility at the same time. However, the pixel size of currently available SLMs limits the achievable numerical aperture (NA) of the SLM displayed diffractive lens to values well below those that can be reached by a refractive lens, implying a strict limit on the resolutions that can be achieved by the prior design. Following, we introduce a new JORDI system that incorporates an additional objective lens. Hence, this system is not limited by the low NA of the SLM.

## 2. System design and theoretical analysis

The proposed JORDI design is schematically presented in Fig. 1(a). The system consists of an objective lens $L_o$, two phase-only SLMs located between two polarizers, and a digital camera [e.g., a charge-coupled device (CCD)]. The two SLMs are positioned with the ordinary/extraordinary axis of *SLM*1 in parallel to the extraordinary/ordinary axis of *SLM*2, meaning that their active axes are perpendicular to each other. The two polarizers, *P*1 and *P*2, are set in parallel to each other, and at a 45° angle to the active axes of the SLMs. This setup can be analyzed by considering each of the two SLMs as affecting orthogonal components of the input wave, as described in Figs. 1(b) and 1(c). A collimated laser beam is used to illuminate a target object (e.g., a resolution test chart) and also serves as a reference, where

#204375 - $15.00 USD Received 8 Jan 2014; revised 11 Feb 2014; accepted 13 Feb 2014; published 24 Feb 2014

the requirement is that some part of the collimated beam arrives to the system input plane unaffected by the target object, thereby forming the joint object reference input plane.

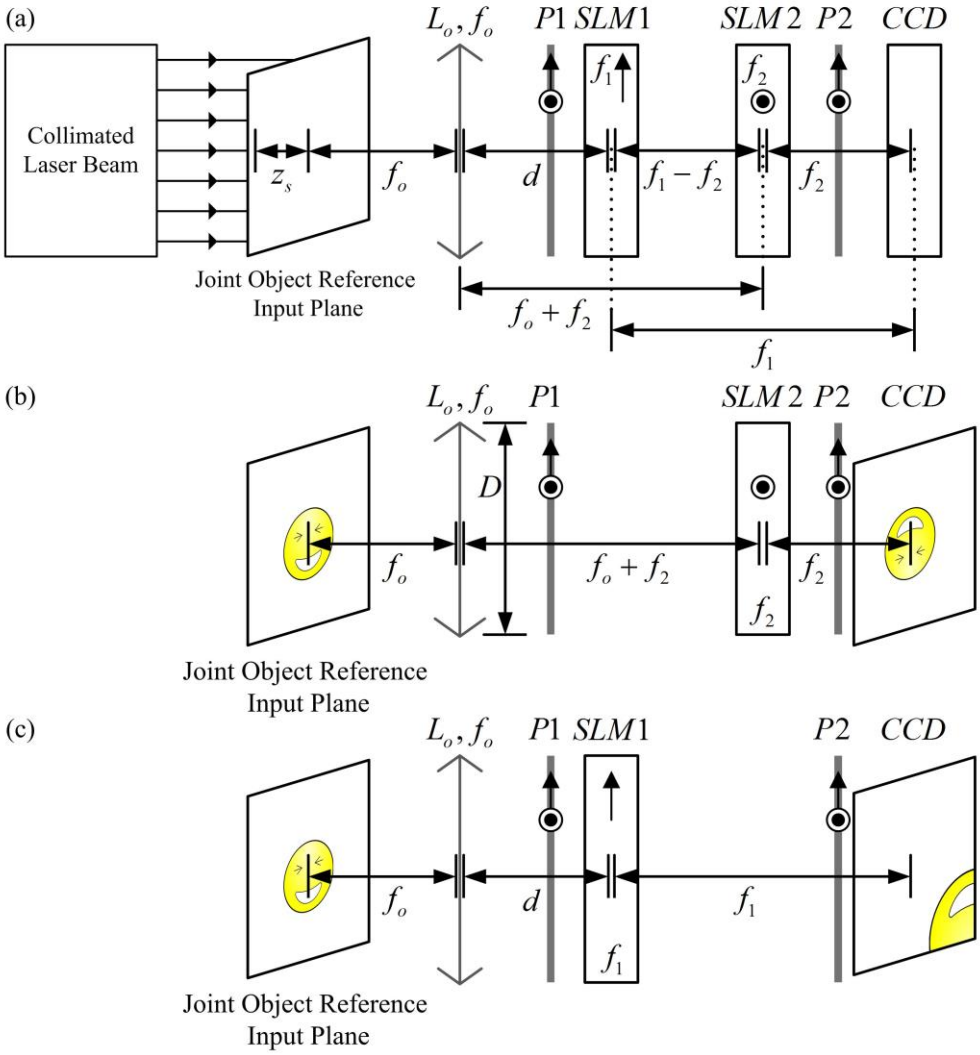


Fig. 1. Schematics of the proposed JORDI design: $L_o$, objective lens; *P*1 and *P*2, polarizers; *SLM*1 and *SLM*2, spatial light modulators; *CCD*, charge-coupled device. In (a) the complete system is presented, whereas in (b) and (c) the imaging systems creating the object and reference waves are presented separately and respectively. The symbols ⊙, ↑, and ⊙↑ are polarization orientations perpendicular, parallel and at a 45° angle to the plane of the page, respectively.

For the object scattered part of the input wave, polarized perpendicularly to the plane of the page, the system acts as an afocal imaging system [Fig. 1(b)] built from two converging lenses: the refractive lens $L_o$ with a focal length of $f_o$ and an additional diffractive lens with a focal length of $f_2$ displayed on *SLM*2. Consider an arbitrary input wave $u_{in}(x, y)$ arriving to the joint object reference input plane of the optical system. Upon arrival to the CCD plane, this wave is:

#204375 - $15.00 USD Received 8 Jan 2014; revised 11 Feb 2014; accepted 13 Feb 2014; published 24 Feb 2014

$$u_{out1}(x,y) = c_1 u_{in}(x,y) * Q\left(\frac{1}{f_o}\right) \cdot Q\left(-\frac{1}{f_o}\right) * Q\left(\frac{1}{f_o + f_2}\right) \cdot Q\left(-\frac{1}{f_2}\right) * Q\left(\frac{1}{f_2}\right), \quad (1)$$

where $Q(s) = \exp[i\pi s\lambda^{-1}(x^2 + y^2)]$ is the quadratic phase function, in which $\lambda$ is defined as the central wavelength of the coherent laser illumination, $*Q(1/z_d)$ denotes a Fresnel propagation of a wave to a distance $z_d$ (mathematically, the $*$ symbol denotes a two-dimensional convolution), $Q(-1/f)$ denotes the influence of a converging lens of a focal length of $f$ and $c_1$ is a complex constant.

For the reference part of the input wave, polarized in parallel to the plane of the page, the system acts as a two-lens imaging system [Fig. 1(c)], realized by the refractive lens $L_o$ and an additional diffractive lens with a focal length of $f_1$, displayed on *SLM*1. Unlike the imaging system of Fig. 1(b), this system is not afocal, and the wave reaching the CCD after passing through it is:

$$u_{out2,k}(x,y) = c_2 e^{i\theta_k} u_{in}(x,y) * Q\left(\frac{1}{f_o}\right) \cdot Q\left(-\frac{1}{f_o}\right) * Q\left(\frac{1}{d}\right) \cdot Q\left(-\frac{1}{f_1}\right) \cdot L\left(\frac{\vec{A}}{f_1}\right) * Q\left(\frac{1}{f_1}\right) \quad (2)$$

where $L(\vec{s}) = \exp[i2\pi\lambda^{-1}(s_x x + s_y y)]$ is the linear phase, with $\vec{s} = (s_x, s_y)$, $c_2$ is a complex constant, and $\exp(i\theta_k)$ denotes an additional phase term that enables the phase-shifting procedure [1], where $\theta_k = 2\pi k/3$, with $k = 0,1,2$. Note that *SLM*1 is used for the realization of the expression $\exp(i\theta_k) \cdot Q(-1/f_1) \cdot L(\vec{A}/f_1)$, which includes the phase-shifting term, a diffractive lens, and an additional linear phase that can be used to achieve lateral displacement of the reference part, controlled by the two dimensional parameter $\vec{A} = (A_x, A_y)$, as shown in Fig. 1(c).

Without loss of generality, assume an input wave of $u_{in}(x,y) = Q(1/z_s)L(-\vec{r}_s/z_s)$ due to a point source located at a distance $z_s$ to the left of the joint object reference input plane [i.e., at a distance of $z_s + f_o$ from the objective lens $L_o$, as seen in Fig. 1(a)], at coordinates $\vec{r}_s = (x_s, y_s)$. Based on a mathematical justification presented in [20], it is easy to show that, for this case, Eq. (1) results with:

$$u_{out1}(x,y) = b_1 L\left[\frac{\frac{f_2}{f_o}\vec{r}_s}{\left(\frac{f_2}{f_o}\right)^2 z_s}\right] Q\left[\frac{1}{\left(\frac{f_2}{f_o}\right)^2 z_s}\right], \quad (3)$$

where $b_1$ is a complex constant. Equation (3) indicates a transverse magnification of $m_{t1} = -f_2/f_o$ and an axial magnification of $m_{a1} = m_{t1}^2 = (f_2/f_o)^2$, which are well-known results for this type of afocal systems [21]. Alternatively, for an arbitrary input wave $u_{in}(x,y)$ Eq. (1) can be rewritten as:

$$u_{out1}(x,y) = a_1 u_{in}\left(\frac{x}{m_{t1}}, \frac{y}{m_{t1}}\right), \quad (4)$$

where $a_1$ is a complex constant.

#204375 - $15.00 USD Received 8 Jan 2014; revised 11 Feb 2014; accepted 13 Feb 2014; published 24 Feb 2014

Regarding the system shown in Fig. 1(c), considering $u_{in}(x,y) = Q(1/z_r)L(-\vec{r}_r / z_r)$ as a reference due to a point source, and applying the relation $d = f_o + 2f_2 - f_1$, Eq. (2) turns into:

$$u_{out2,k}(x,y) = b_2 e^{i\theta_k} L\left(\frac{-\vec{A}}{\frac{f_1^2}{f_1 - 2f_2}}\right) Q\left[\frac{1}{\frac{f_1^2}{2(f_1 - f_2)}}\right] L\left[\frac{\frac{f_1}{f_o}\vec{r}_r - \vec{A}}{\left(\frac{f_1}{f_o}\right)^2 z_r}\right] Q\left[\frac{1}{\left(\frac{f_1}{f_o}\right)^2 z_r}\right], \quad (5)$$

where $b_2$ is a complex constant. The two right-most terms in Eq. (5) indicate a transverse magnification of $m_{t2} = -f_1 / f_o$, an axial magnification of $m_{a2} = m_{t2}^2 = (f_1 / f_o)^2$, and a lateral displacement away from the optical axis of $\vec{A}$, so that for an arbitrary input wave $u_{in}(x,y)$ Eq. (5) can be rewritten as:

$$u_{out2,k}(x,y) = a_2 e^{i\theta_k} L\left(\frac{-\vec{A}}{\frac{f_1^2}{f_1 - 2f_2}}\right) Q\left[\frac{1}{\frac{f_1^2}{2(f_1 - f_2)}}\right] u_{in}\left(\frac{x - A_x}{m_{t2}}, \frac{y - A_y}{m_{t2}}\right), \quad (6)$$

where $a_2$ is a complex constant.

Assume that the object and reference parts of the input wave occupy the regions $\Omega_{in,obj}$ and $\Omega_{in,ref}$ inside the joint object reference input plane, respectively. Based on Eq. (4) and Eq. (6), $\Omega_{out,obj}$ and $\Omega_{out,ref}$, the regions of the object and reference parts on the output plane of the system, respectively, can easily be identified. Successful hologram recording requires the object region $\Omega_{out,obj}$ to be contained within the reference region $\Omega_{out,ref}$ (i.e., with $\Omega_{out,obj} \subseteq \Omega_{out,ref}$), a condition which can be satisfied by a proper selection of the parameters $m_{t1}$, $m_{t2}$ and $\vec{A}$, where the first two are used to ensure that $\Omega_{out,ref}$ is large enough to contain $\Omega_{out,obj}$, and the latter controls the displacement of $\Omega_{out,ref}$ so that it overlaps $\Omega_{out,obj}$.

Now, let us consider the case where the parameters $m_{t1}$, $m_{t2}$ and $\vec{A}$ are indeed chosen so that the object and reference parts of the same input wave overlap each other on the CCD plane [Figs. 1(b) and 1(c)]. For simplicity, further assume that the focal length $f_1$ is chosen to be equal twice the focal length $f_2$ (i.e., $f_1 = 2f_2$). A reasoning based on Eqs. (4)–(6), which is detailed in the Appendix, shows that the intensity inside the region $\Omega_{out,obj}$, recorded by the CCD, is:

$$I_k(x,y) = \left|u_{out1}(x,y) + u_{out2,k}(x,y)\right|^2 = \left|a_1 u_{in}\left(\frac{x}{m_{t1}}, \frac{y}{m_{t1}}\right) + a_2 e^{i\theta_k} Q\left(\frac{1}{f_1}\right)\right|^2, \forall (x,y) \in \Omega_{out,obj}. \quad (7)$$

Following a phase-shifting procedure described in [1], a complex-valued digital hologram is formed:

$$H(x,y) \propto u_{in}\left(\frac{x}{m_{t1}}, \frac{y}{m_{t1}}\right) \cdot Q\left(-\frac{1}{f_1}\right), \forall (x,y) \in \Omega_{out,obj}, \quad (8)$$

#204375 - $15.00 USD Received 8 Jan 2014; revised 11 Feb 2014; accepted 13 Feb 2014; published 24 Feb 2014

where the term $u_{in}(x/m_{t1}, y/m_{t1})$ represents the recorded amplitude and phase information of the input object wave, and $Q(-1/f_1) = Q^*(1/f_1)$ is a conjugated phase term attributed to the reference. Note that this last term does not contain any object related information, and its parameters are determined by the physical properties of the optical setup. As such, it can be digitally eliminated, although this step is usually not essential. Further note that in order to achieve balance between the object and the reference waves it is possible to set the two polarizers, *P*1 and *P*2, at angles which are different from the previously mentioned 45°.

Consider an object located at the joint object reference plane of the imaging system presented in Fig. 1(b) (i.e., at the front focal plane of the objective lens $L_o$). According to the Abbe resolution criterion [22], the minimum resolvable distance between a pair of grating lines at the input plane of a coherent imaging system is $\Delta_{min} = 0.82 \cdot \lambda / NA$, where $NA \simeq D/2f_o$ is the numerical aperture of the system. The parameter $D$ represents the system aperture size [Fig. 1(b)], determined either by the diameter of objective lens $L_o$ or by the height of the SLM that is being used (the smaller of these two sizes), and $f_o$ represents the focal length of the objective lens $L_o$. The resolution of the imaging system presented in Fig. 1(c) is similar, but of lesser importance, since the spatial bandwidth of the reference part of the input wave is much smaller than the bandwidth of the object wave. However, the fringe patterns formed by the interference of these two waves should be faithfully recorded by the CCD. The maximal spatial frequency of such a pattern can be found based on geometrical considerations. Under the assumption that both the CCD and *SLM*2 are limited to an aperture of the size $D$, the maximal possible angle of an object wave reaching the CCD is given by $\alpha_{1,max} = \arctan(D/f_2) = \arctan(2NA/|m_{t1}|)$. As implied by the quadratic phase term $Q(1/f_1)$ in Eq. (7), the reference wave reaches the CCD with a maximal angle of $\alpha_{2,max} = \arctan(0.5D/f_1) = \arctan(0.5NA/|m_{t1}|)$. Under the paraxial approximation, the interference pattern of these two waves is limited to a maximal spatial frequency of $f_{max} = (\alpha_{1,max} - \alpha_{2,max})/\lambda \simeq 1.5NA/(\lambda \cdot |m_{t1}|)$ (note that $\alpha_{1,max} - \alpha_{2,max}$ is the largest possible interference angle between the waves, calculated at the edge of the CCD plane). Accordingly, the pixel size of the digital camera, $\Delta_p$, should satisfy the relation $2\Delta_p \le |m_{t1}| \cdot 0.67 \cdot \lambda / NA$, or else the system resolution might be diminished. Nevertheless, whenever this relation is met, the system resolution is determined by the aforementioned Abbe resolution criterion for coherent imaging systems with:

$$\Delta_{min} = 0.82 \cdot \frac{\lambda}{NA} = \frac{1.64 \cdot f_o \lambda}{D}. \tag{9}$$

Note that the hologram sampling condition, $\Delta_p \le (|m_{t1}|/2) \cdot (0.67 \cdot \lambda / NA) = 0.67 \cdot \lambda f_2 / D$, can easily be satisfied by choosing $f_2$ large enough, assuring finest achievable resolution.

### 3. Experiments and results

We implemented a JORDI system as shown in Fig. 2. This implementation is based on Fig. 1(a), but since the two SLMs are reflective, beam splitters were placed in front of each of them, aligning their planes perpendicularly to the optical axis. We note that for light demanding applications one can avoid using the beam splitters, and instead, position the SLMs at an angle to the optical axis while applying corrections to the SLM displayed elements (see, for example [1,2]). For imaging of samples that might be damaged by an excessive amount of light it may be beneficial to position the polarizer *P*1 before the sample, or simply use a weaker linearly polarized laser, assuming the influence of the sample on the

#204375 - $15.00 USD Received 8 Jan 2014; revised 11 Feb 2014; accepted 13 Feb 2014; published 24 Feb 2014

beam polarization is negligible. In the experiments, two identical Holoeye PLUTO SLMs (1920x1080 pixels, 8μm pixel pitch, phase only modulation) and either an Allied Vision Technologies Prosilica GT2750 CCD (2750x2200 pixels, 4.54μm pixel pitch, monochrome) or a PixelFly CCD (1280x1024 pixels, 6.7μm pixel pitch, monochrome) were used. The focal lengths of the diffractive lenses realized on *SLM*1 and *SLM*2 were set to $f_1 = 40cm$ and $f_2 = 20cm$, respectively. The illumination source was a collimated red HeNe laser ($\lambda = 632.8$nm, 5mW).

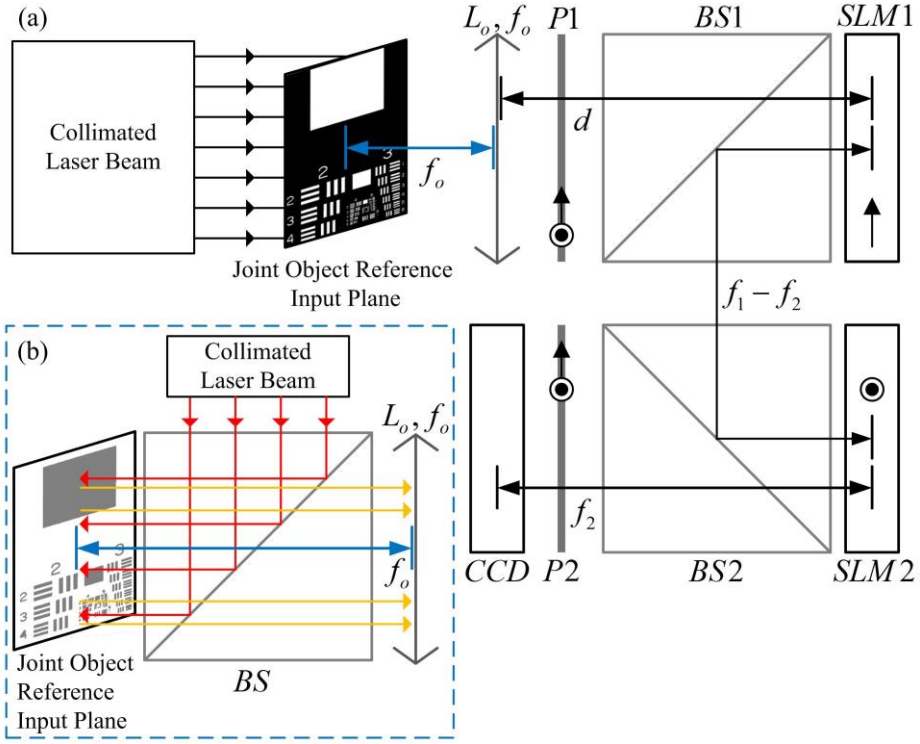


Fig. 2. Experimental setup of JORDI: $L_o$, objective lens; *P*1 and *P*2, polarizers; *BS*1 and *BS*2, beam splitters; *SLM*1 and *SLM*2, spatial light modulators; *CCD*, charge-coupled device. The symbols ⊙, ↑, and ⇕ are polarization orientations perpendicular, parallel and at a 45° angle to the plane of the page, respectively. The setup in (a) is suitable for recording transmissive objects, whereas the alternative illumination configuration demonstrated in (b) enables recording reflective objects.

In the first experiment, a plano-convex refractive lens with a focal length of $f_o = 17.5cm$ served as the objective lens $L_o$, located at a distance $d = f_o = 17.5cm$ from *SLM*1. A negative 1951 USAF resolution test target (Thorlabs R3L3S1N) was placed $18.5cm$ away from $L_o$. Resolution groups 2 (elements 2 to 4) and 3 to 7 (all elements) served as the target, whereas the empty square located above these two groups served as a free passing region for the reference [see Fig. 2(a)]. The amplitude and phase of the recorded JORDI hologram are presented in Figs. 3(a) and 3(b), respectively. Its reconstruction is presented in Fig. 3(c), where a Fresnel back propagation to a distance of $z_r \simeq 1.34cm$ was used to achieve best focus. Note that the reconstruction distance is affected by the reference term $Q(-1/f_1)$, though its influence is small when $|f_1| \gg |z_r|$. Average cross-sections of elements 1 to 4 of resolution group 5, which are highlighted in Fig. 3(c), are shown in Figs. 3(d)–3(g),

#204375 - $15.00 USD Received 8 Jan 2014; revised 11 Feb 2014; accepted 13 Feb 2014; published 24 Feb 2014

respectively, and indicate that the resolution of the holography system is better than 40.3 line pairs per millimeter (lp/mm) (for element 3 of group 5), where the distance between the centers two bright lines (i.e., the width of two single lines) is $\Delta = 24.81\mu m$. However, at 45.3 lp/mm (for element 4 of group 5), with $\Delta = 22.08\mu m$, the visibility is significantly lower and the resolution of the system is barely sufficient to resolve details. Comparing this result to the resolution limit indicated by the Abbe criterion [Eq. (9)], $\Delta_{min} = 0.82 \cdot \lambda / NA \simeq 22.22\mu m$, with a numerical aperture of $NA \simeq D/2(f_o + z_s) = 1080 \cdot 8 \cdot 10^{-6} / [2 \cdot (0.175 + 0.01)] \simeq 23.35 \cdot 10^{-3}$, indicates that indeed, the resolution of the proposed system matches the theoretical limit. Note that in the presented case, the pixel size of the digital camera does not limit the resolution of the system [Eq. (9)].

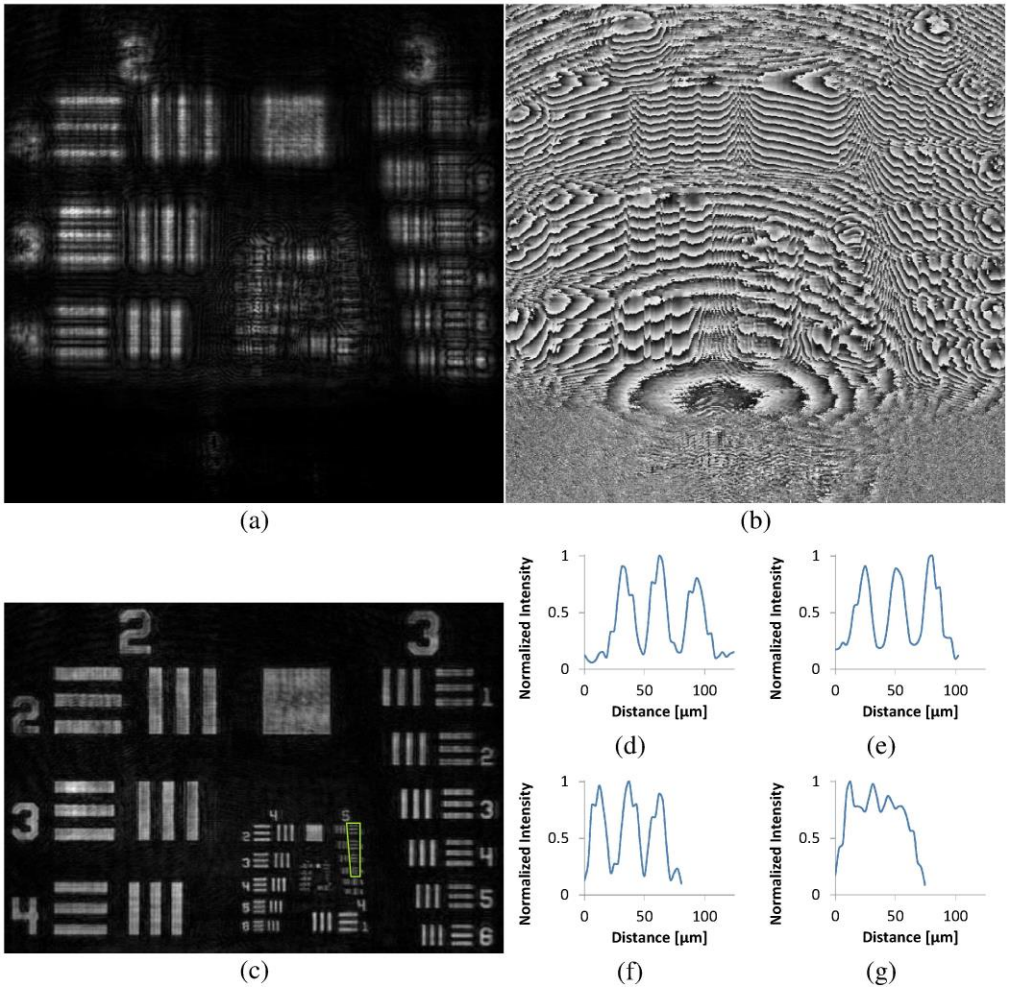


Fig. 3. JORDI recording of a transmissive target: (a) amplitude and (b) phase of the recorded hologram; (c) hologram reconstruction at the plane of best focus; (d)-(g) cross sections of elements 1 to 4 of group 5 (highlighted) of the resolution targets, respectively.

In the second experiment, the test target was replaced with a positive 1951 USAF resolution test target (Thorlabs R3L3S1P) in order to demonstrate the system operation with a highly reflective object. Similarly to the previous experiment, resolution groups 2 (elements 2 to 4) and 3 to 7 (all elements) served as the target, whereas the square located above these two groups served as a mirror for the reference. This time, the collimated laser beam was used to

#204375 - $15.00 USD Received 8 Jan 2014; revised 11 Feb 2014; accepted 13 Feb 2014; published 24 Feb 2014

illuminate the target from its front, instead of its back, using a beam-splitter, as shown in Fig. 2(b). Other parameters of the experimental setup were left unchanged. The amplitude and phase of the recorded hologram are presented in Figs. 4(a) and 4(b), respectively, with its reconstruction in Fig. 4(c), where a Fresnel back propagation was used to achieve the best focus. An enlarged portion of the reconstruction, for resolution groups 4 and above, is shown in Fig. 4(d). Comparing Fig. 4(d) to the transmissive target results (Fig. 3), shows that in terms of resolution, both cases lead to similar results. However, background artifacts are much more prominent in the case of the reflective object, and are the result of the reflectivity of the non-mirrored parts of the glass made 1951 USAF target. In the previous experiment, light had been able to pass only through clear parts of the target, while here there was a strong reflection from the lines and figures and an additional weak reflection elsewhere.

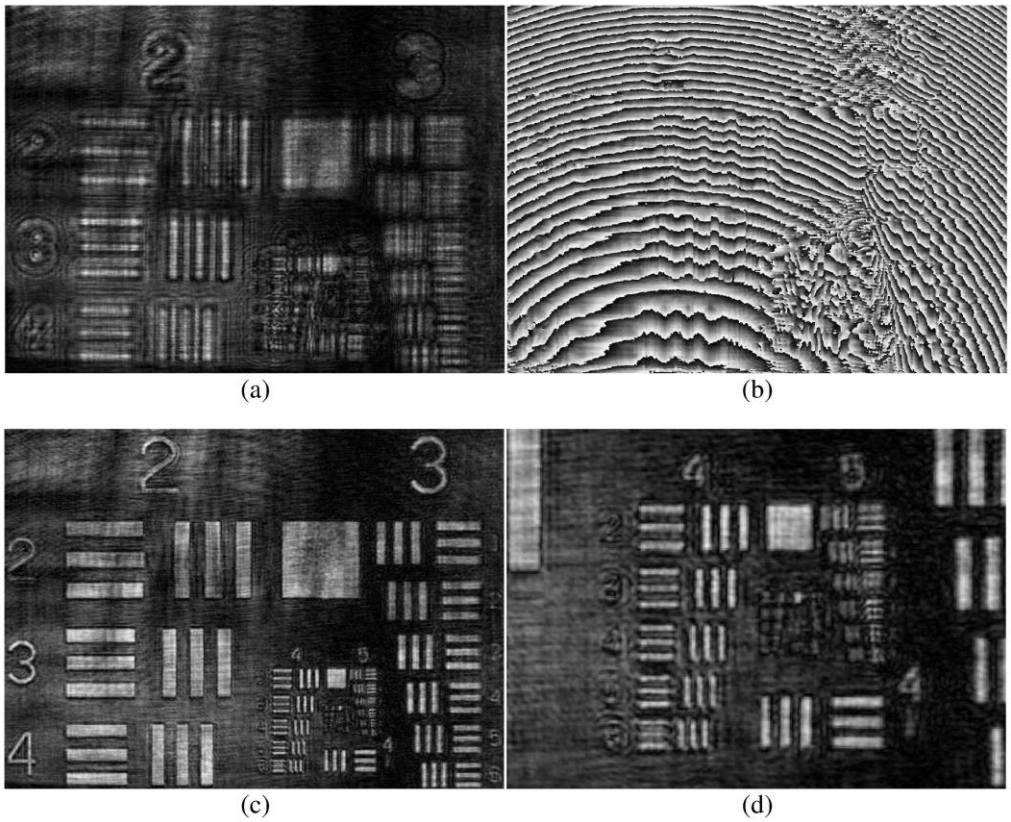


Fig. 4. JORDI results for a reflective target: (a) amplitude and (b) phase of the recorded hologram; (c) hologram reconstruction at the plane of best focus; (d) enlarged portion of (c) shows details of resolution groups 4 and 5.

The third experiment demonstrates the system capability of recording holograms of a three-dimensional scene. Two transmissive targets were placed roughly 1cm away from each other: a 4.0 cycles/mm group of a positive NBS 1963A resolution test target and a 'X1' inscription from a positive 1951 USAF resolution test target. The amplitude and phase of the recorded hologram are presented in Figs. 5(a) and 5(b), respectively. Figures 5(c) and 5(d) demonstrate the preservation of the three-dimensional information of the scene, with the 4.0 cycles/mm and 'X1' inscriptions in the best focus, respectively. Note that in Fig. 5(b) the phase of the reference beam was digitally eliminated based on Eq. (8), in order to emphasize phase details from the actual objects. This manipulation does not affect the quality of the hologram reconstructions [Figs. 5(c) and 5(d)] and nor is essential. However, it does influence the reconstruction distance to a small degree.

#204375 - $15.00 USD Received 8 Jan 2014; revised 11 Feb 2014; accepted 13 Feb 2014; published 24 Feb 2014

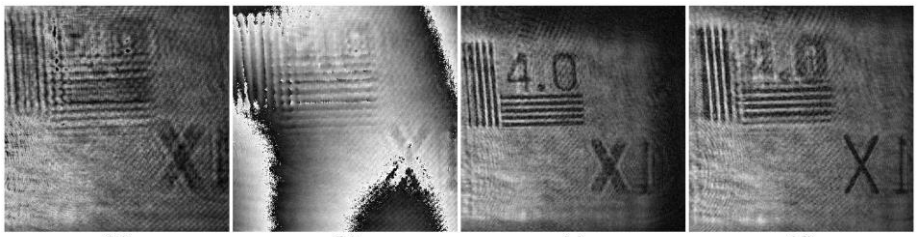


(a) (b) (c) (d)

Fig. 5. JORDI recording of a three-dimensional scene: (a) amplitude and (b) phase (shown after eliminating the quadratic phase term of the reference) of the recorded Fresnel hologram; (c) hologram reconstruction at the plane of best focus of the 4.0 cycles/mm inscription; (d) hologram reconstruction at the plane of best focus of the 'X1' inscription.

The fourth experiment demonstrates the system capability of recording holograms of reflective, highly scattering objects. An Israeli 5 Agorot coin (withdrawn from circulation in 2008) has been used as the target object. The coin was placed in front of a reflective neutral density filter that allowed part of the collimated laser to serve as a reference beam of controllable intensity. To extend the field of view, an afocal system of −1/4x magnification was inserted between the object and the system entrance lens $L_o$, with $f_a = 30cm$ and $f_b = 7.5cm$ [see Fig. 6(a)]. Experimental results are presented in Figs. 6(b)–6(d). While the amplitude of the recorded hologram [Fig. 6(b)] exposes only few details of the out-of-focus coin, the additional phase information [Fig. 6(c)] enables focusing into the coin [Fig. 6(d)], where much more details are visible, including the digit '5′.

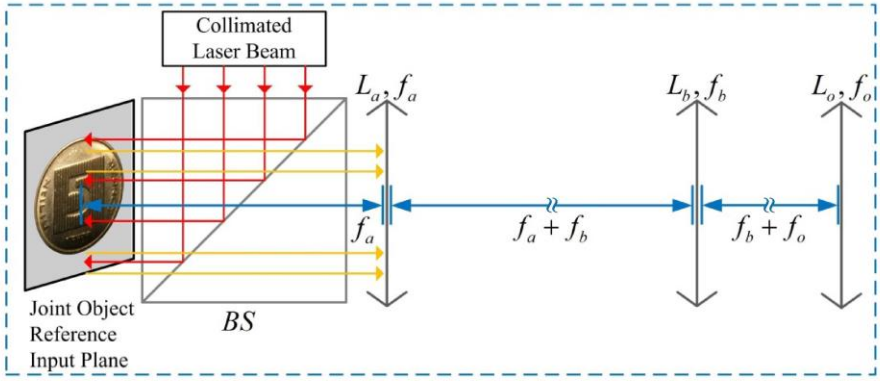


(a)

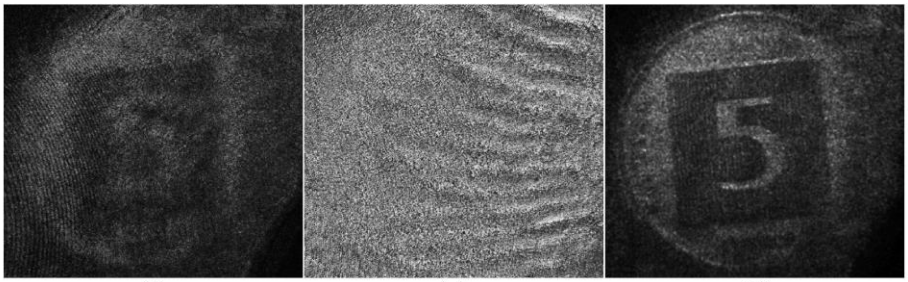


(b) (c) (d)

Fig. 6. JORDI results for a highly scattering object: (a) modification of the experimental setup (Fig. 2), where a relay system of –1/4x magnification, realized by the lenses $L_a$ and $L_b$, extends the field of view of the system; (b) amplitude and (c) phase of the recorded hologram, where out-of-focus details of the Israeli 5 Agorot coin are barely visible; (d) hologram reconstruction at the plane of best focus, exposing details of the 5 Agorot coin.

#204375 - $15.00 USD Received 8 Jan 2014; revised 11 Feb 2014; accepted 13 Feb 2014; published 24 Feb 2014

In the fifth experiment, the applicability of the proposed system for microscopy is demonstrated using a microscope objective (Newport M-10X, 0.25 NA, $f_o = 16.5mm$) lens as $L_o$. The focal lengths of the two SLM realized diffractive lenses were $f_1 = 40cm$ and $f_2 = 20cm$ for *SLM*1 and *SLM*2, respectively. Groups 6 and 7 of a negative 1951 USAF resolution test target (Thorlabs R3L3S1N), served as an object, and the square between group 4 (element 2) and group 5 (element 1) of the same target was used as a reference. The amplitude and phase of the recorded hologram are shown in Figs. 7(a) and 7(b), respectively, with its reconstruction at plane of focus in Fig. 7(c). All groups and elements are clearly visible, including element 6 of group 7, implying a lateral resolution of at least $\Delta = 4.38\mu m$. Note that Eq. (9) indicates an achievable resolution of $\Delta_{min} \simeq 2.08\mu m$.

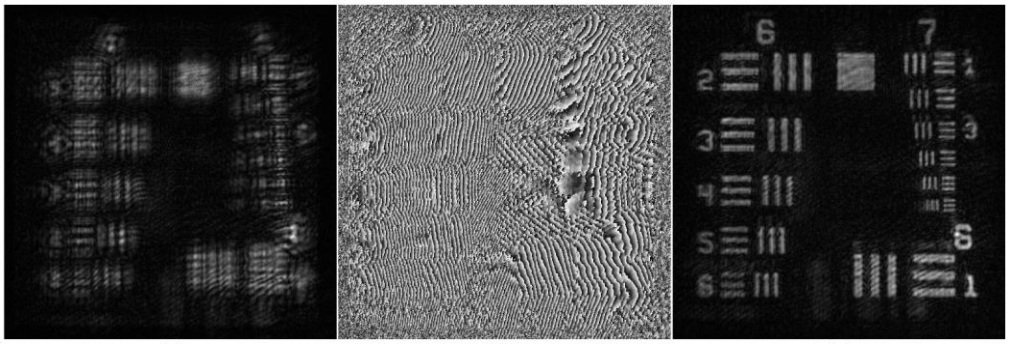


(a) (b) (c)

Fig. 7. JORDI based holographic microscopy: (a) amplitude and (b) phase of the recorded hologram; (c) hologram reconstruction at the plane of best focus, showing complete details of resolution groups 6 and 7, up to 228 lp/mm.

In order to further justify the suitability of the proposed system for microscopy, the system capability of recording holograms of phase objects was verified. The configuration of the first experiment was used together with a plano-convex cylindrical lens (Newport CKX300, N-BK7 made, effective focal length $f_c = 30cm$) as a test target, located $17.5cm$ away from $L_o$. The amplitude of the recorded hologram is shown in Fig. 8(a). In Figs. 8(b) and 8(c) the wrapped and unwrapped phase profiles of the cylindrical lens [magnified by the imaging system of Fig. 1(b)] are shown, respectively, after the phase of the reference beam has been digitally eliminated according to Eq. (8). In Fig. 8(d) the measured phase profile of the lens at a fixed x-axis position of $x = -1mm$ along the y-axis is shown together with the theoretical profile calculated according to $\phi(y) = -2 \cdot (n-1) \cdot \pi / \lambda \cdot [r - (r^2 - y^2)^{(1/2)}]$, where $n = 1.515$ is the refractive index of N-BK7 and $r = m_{a1} f_c (n-1)$ [21]. Some variations are evident between the two curves, but once an average phase profile is considered, as in Fig. 8(e), the two curves become very similar. It should be also noted that the hologram presented in Fig. 8 is the only image hologram in this study, whereas the other holograms herein are Fresnel holograms.

#204375 - $15.00 USD Received 8 Jan 2014; revised 11 Feb 2014; accepted 13 Feb 2014; published 24 Feb 2014

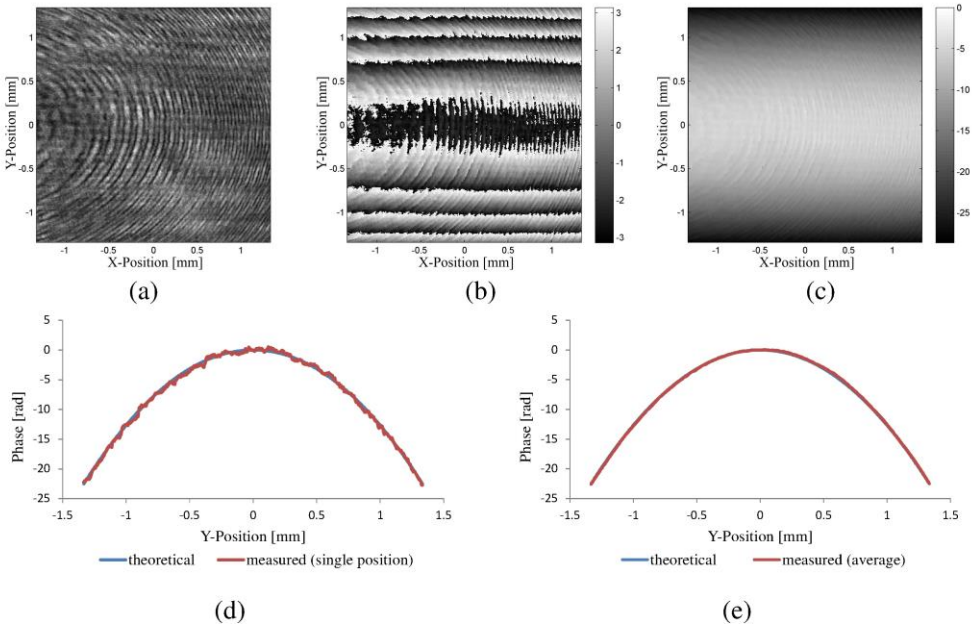


Fig. 8. JORDI recording of a phase target: (a) amplitude and (b) wrapped phase of the recorded hologram; (c) unwrapped phase profile of (b); (d) theoretical and measured (after phase unwrap and bias elimination) phase profiles at X-Position = 1mm; (e) theoretical and average measured phase profiles.

## 4. Summary and conclusions

A new holographic system based on the JORDI concept has been presented. In the previous JORDI implementation [1], each of the two SLMs functioned as a single lens imaging system, and so the resolution of the system was limited by the relatively low numerical apertures that can be achieved using currently available SLMs. The proposed enhanced system, however, is not limited by this factor and a higher resolution can be achieved using an objective lens of a higher numerical aperture.

We have successfully demonstrated the recording of various holograms using transmissive, reflective, three-dimensional, highly scattering and phase objects. The analysis of the experimental results indicates that the achieved resolutions are similar to those implied by the Abbe resolution criterion for coherent imaging systems. In addition, by incorporating a microscope objective into the proposed setup, a hologram of a transmissive resolution test target capable of distinguish details as small as $4.38\mu m$ was recorded, indicating the applicability of JORDI in the microscopy regime.

## Appendix

In this appendix the derivation of Eq. (7) is explained. Without loss of generality, assume that the object part of the input wave $u_{in}(x,y)$ is constrained into a rectangular region $\Omega_{in,obj}$ of size $w_{x,obj} \times w_{y,obj}$ on the joint object reference xy-plane, with its center located at the coordinate $(x_{c,obj}, y_{c,obj})$. Further assume that the reference part of the input wave, unscattered by the object, occupies a rectangular region $\Omega_{in,ref}$ of size $w_{x,ref} \times w_{y,ref}$, with its center located at the coordinate $(x_{c,ref}, y_{c,ref})$. In this case, the object part of the input wave can be expressed as:

#204375 - $15.00 USD Received 8 Jan 2014; revised 11 Feb 2014; accepted 13 Feb 2014; published 24 Feb 2014

$$u_{in,obj}(x,y) = u_{in}(x,y)\,rect\left(\frac{x-x_{c,obj}}{w_{x,obj}}, \frac{y-y_{c,obj}}{w_{y,obj}}\right), \tag{10}$$

while the reference part of the input wave can be expressed as:

$$u_{in,ref}(x,y) = u_{in}(x,y)\,rect\left(\frac{x-x_{c,ref}}{w_{x,ref}}, \frac{y-y_{c,ref}}{w_{y,ref}}\right), \tag{11}$$

where $rect(x,y)$ is the rectangular function, here defined as:

$$rect(x,y) = \begin{cases} 1 & \text{for } |x| \le 1 \text{and} |y| \le 1 \\ 0 & \text{elsewhere} \end{cases}. \tag{12}$$

We emphasis that the object and reference parts of the input wave are here confined to rectangular regions for the sake of simplicity, and in general this restriction is not necessarily met.

According to Eq. (4) and Eq. (10), the object part of the wave reaching the CCD is:

$$u_{out,obj}(x,y) = a_1 u_{in}\left(\frac{x}{m_{t1}}, \frac{y}{m_{t1}}\right) rect\left(\frac{x-m_{t1}x_{c,obj}}{m_{t1}w_{x,obj}}, \frac{y-m_{t1}y_{c,obj}}{m_{t1}w_{y,obj}}\right). \tag{13}$$

The reference part of the wave reaching the CCD is found in accordance to Eq. (6) and Eq. (11):

$$\begin{aligned} u_{out,k,ref}(x,y) = a_2 e^{i\theta_k} Q\left(\frac{1}{f_1}\right) u_{in}\left(\frac{x-A_x}{m_{t2}}, \frac{y-A_y}{m_{t2}}\right) \\ \cdot rect\left[\frac{x-\left(m_{t2}x_{c,ref}+A_x\right)}{m_{t2}w_{x,ref}}, \frac{y-\left(m_{t2}y_{c,ref}+A_y\right)}{m_{t2}w_{y,ref}}\right]. \end{aligned} \tag{14}$$

Note that in deriving Eq. (14) the previously mentioned relation of $f_1 = 2f_2$ is assumed. By taking Eq. (5) with $z_r \to \infty$ and $\vec{r}_r = \vec{0}$, the collimated laser beam [Fig. 1(a)] acts as the reference source. Equation (14) is then easily simplified into:

$$u_{out,k,ref}(x,y) = a_2 e^{i\theta_k} Q\left(\frac{1}{f_1}\right) rect\left[\frac{x-\left(m_{t2}x_{c,ref}+A_x\right)}{m_{t2}w_{x,ref}}, \frac{y-\left(m_{t2}y_{c,ref}+A_y\right)}{m_{t2}w_{y,ref}}\right]. \tag{15}$$

Based on Eq. (13) and Eq. (15), whenever the condition

$$\left|\frac{m_{t2}}{m_{t1}}\right| \ge \max\left\{\frac{w_{x,obj}}{w_{x,ref}}, \frac{w_{y,obj}}{w_{y,ref}}\right\} \tag{16}$$

is satisfied, the rectangular area of $\Omega_{out,obj}$ can be contained inside $\Omega_{out,ref}$ (i.e., $\Omega_{out,obj} \subseteq \Omega_{out,ref}$), by controlling the displacement of $\Omega_{out,ref}$ via the parameter $\vec{A} = (A_x, A_y)$.

In this specific example, we have chosen $f_1 = 2f_2$ so that $|m_{t2}/m_{t1}| = f_1/f_2 = 2$, and the condition in Eq. (16) can be satisfied even when $\Omega_{in,ref}$ is half the size of $\Omega_{in,obj}$. The two regions, $\Omega_{out,obj}$ and $\Omega_{out,ref}$, can then be centered to the same coordinate by selecting the parameter $\vec{A}$ as:

#204375 - $15.00 USD Received 8 Jan 2014; revised 11 Feb 2014; accepted 13 Feb 2014; published 24 Feb 2014

$$\vec{A} = (A_x, A_y) = (m_{t1} x_{c,obj} - m_{t2} x_{c,ref}, m_{t1} y_{c,obj} - m_{t2} y_{c,ref}). \quad (17)$$

Note that while Eq. (17) suggests a satisfactory selection of $\vec{A}$, in certain cases the selection of smaller absolute values of $A_x$ and $A_y$ may be possible, and the above solution is discussed here for the sake of brevity. Once the conditions of Eq. (16) and Eq. (17) are fulfilled, $\Omega_{out,obj} \subseteq \Omega_{out,ref}$, and the rectangular function terms in Eq. (13) and Eq. (15) are simply equal to one for every $(x, y) \in \Omega_{out,obj}$. The recoded intensity of the interference between these reference and object waves in this region is then given by Eq. (7).

**Acknowledgments**

We thank Yair Rivenson for his contribution to the initial development of JORDI and for his valuable comments. This work was supported by The Israel Ministry of Science and Technology (MOST), by The Israel Science Foundation (ISF) and by NIH Grant U54GM105814.

#204375 - $15.00 USD Received 8 Jan 2014; revised 11 Feb 2014; accepted 13 Feb 2014; published 24 Feb 2014